

Replication-related control over cell division in *Escherichia coli* is growth-rate dependent

Sriram Tiruvadi-Krishnan^{1*}, Jaana Männik^{1*}, Prathitha Kar^{2,3}, Jie Lin^{2,4}, Ariel Amir², Jaan Männik¹

¹*Department of Physics and Astronomy, University of Tennessee, Knoxville, TN 37996, USA*

²*John A. Paulson School of Engineering and Applied Sciences, ³Department of Chemistry and Chemical Biology, Harvard University, Cambridge, MA 02134, USA*

⁴*Center for Quantitative Biology and Peking-Tsinghua Joint Center for Life Sciences, Academy for Advanced Interdisciplinary Studies, Peking University, Beijing, China*

Corresponding authors: Jaan Männik; JMannik@utk.edu; phone: +1 (865) 974 6018

Ariel Amir; arielamir@seas.harvard.edu; phone: +1 (617) 495-5818

* - Equal contribution

Summary

1 How replication and division processes are coordinated in the cell cycle is a fundamental yet poorly
2 understood question in cell biology. In *Escherichia coli* different data sets and models have supported a
3 range of conclusions from one extreme where these two processes are tightly linked to another extreme
4 where these processes are completely independent of each other. Using high throughput optical
5 microscopy and cell cycle modeling, we show that in slow growth conditions replication and division
6 processes are strongly correlated, indicating a significant coupling between replication and division. This
7 coupling weakens as the growth rate of cells increases. Our data suggest that the underlying control
8 mechanism in slow growth conditions is related to unreplicated chromosome blocking the onset of
9 constriction at the midcell. We show that the nucleoid occlusion protein SlmA does not play a role in this
10 process and neither do other known factors involved in positioning bacterial Z-ring relative to the
11 chromosome. Altogether this work reconciles different ideas from the past and brings out a more nuanced
12 role of replication in controlling the division process in a growth-rate dependent manner.

13

14 **Keywords:** cell cycle checkpoint, cell division, FtsN, cell cycle modeling, *Escherichia coli*, microfluidics

15 **Introduction**

16 The studies addressing coordination between DNA replication and cell division cycles in *Escherichia coli*
17 date back more than half a century and are still being strongly influenced by the classic Cooper-
18 Helmstetter (CH) model [1]. The latter postulates that cell division completes a period of constant
19 duration, referred to as D-period, after the termination of replication. The model also proposed that the
20 replication period C is growth rate independent in a range of faster growth rates. A constant D-period,
21 which was found to be independent of the growth rate in faster growth rates, would imply that cell
22 division is tightly coupled to replication termination. These predictions have been revisited more recently
23 using single-cell measurements. A good match between the CH model and data was found but only under
24 a further assumption that the C+D period depends on the growth rate in a specific way [2].

25 As a new element for cell cycle control going beyond the CH model, the adder concept has been
26 introduced [3-7]. In the adder model cells add a constant volume increment during the cell cycle
27 irrespective of their size at birth. In some of these models, the increment is assumed to be added between
28 two consecutive replication events, and cell division is still thought to be tightly coupled to replication [3,
29 6, 7]. In others, the increment is added from cell birth to division [4, 5, 8]. In these latter models,
30 replication does not play any role in the division process. The latter conclusion has also been drawn by
31 some experimental works which have not relied on cell cycle modeling [9, 10]. As the middle ground of
32 these opposing views, Micali *et al.* have proposed a model postulating that division is controlled
33 concurrently by replication and division-related processes; whichever of these processes completes the
34 latest will trigger cell division [11, 12]. In this concurrent-processes model replication and division related
35 processes are competing with each other in triggering cell division in all growth conditions.

36 Cell division occurs when two daughter cells separate from each other. This event can be determined from
37 single-cell time-lapse measurements. The existing models predict the timing and cell sizes at this event.

38 However, it is well-known that the separation of daughter cells results from a long sequence of
39 biochemical processes that only culminate with the separation of two daughter cells [13, 14]. The question
40 arises on what initiates this process sequence and how this initiation is linked to the replication cycle of
41 the chromosome. Previous research has identified that cell division in *E. coli* progresses via two distinct
42 stages [15]. The first of these is the formation of the Z-ring at the cell center. This comprises the assembly
43 of FtsZ protofilaments in the mid-cell region [16]. In *E. coli* the protofilaments are linked to the cell
44 membrane by FtsA and ZipA linkers and likely bundled together with ZapA and several other cross-linking
45 proteins [14, 16]. At multi-forked fast growth conditions, the Z-ring forms at cell birth but in slower growth
46 conditions there is a delay between cell birth and Z-ring formation, which is at least in part controlled by
47 the availability of FtsZ [17, 18]. The Z-ring subsequently recruits about 30 different proteins that are
48 involved in septal cell wall synthesis and partitioning of DNA between daughter compartments [19, 20].
49 The recruitment of these mostly regulatory proteins proceeds in specific order culminating with the
50 recruitment of FtsN to the divisome complex [14, 16, 19, 21-23]. It is hypothesized that FtsN relieves
51 inhibition or activates core septal peptidoglycan synthesis complex consisting of transpeptidase (FtsW)
52 and transglycosylase (FtsI/PBP IIIA) units [24]. There is a significant delay between the formation of the Z-
53 ring and the onset of constriction [15]. The latter was found to be simultaneous with the recruitment of
54 FtsN to the divisome [22]. It is currently unclear why Z-rings form much earlier than constriction is
55 initiated. Furthermore, the experimental studies related to molecular aspects of cell division have not
56 addressed the question of how the recruitment of divisome components is regulated by the replication
57 cycle of the chromosome.

58 Here, we study how the initiation of constriction is controlled by the replication cycle. We use quantitative
59 high-throughput fluorescent microscopy and a new functional endogenous FtsN construct. The latter
60 allows us to accurately determine the timing for constriction formation. Our data and cell cycle modeling
61 are consistent with an idea that replication is a rate-limiting factor for constriction in slow growth

62 conditions. However, the limiting role of replication weakens at faster growth rates. Our results
63 furthermore suggest that the onset of constriction is limited by the unreplicated chromosome at the
64 midcell. This limitation is not related to the nucleoid occlusion factor SlmA, the Ter linkage proteins (ZapA,
65 ZapB, and MatP), and FtsK, a DNA translocase.

66

67 **Results**

68 **Constriction formation follows replication termination in different growth conditions.**

69 To understand the link between replication and division cycles we constructed *E. coli* strains where
70 fluorescent fusion proteins labeled both the replisome and the divisome (for details see Materials and
71 Methods, SI Table S1). We used the N-terminal fusion of mCherry to DnaN (beta clamp) [25] or C-terminal
72 fusion of Ypet to ssb (single-strand binding protein) to label the replisome [26]. For the divisome label, we
73 chose FtsN because it is the latest known component to assemble to the divisome and its recruitment has
74 been reported to coincide with the onset of constriction [14, 16, 19, 21-23]. While in previous fluorescent
75 constructs of FtsN the labeled protein was expressed from extra copy plasmids [19, 27, 28], in our
76 construct it was expressed from the native locus. We grew these strains in steady-state conditions in
77 mother machine devices [29, 30]. The doubling times and lengths of these cells were indistinguishable
78 from the WT ones (strain BW27783) when grown in a glycerol medium (Table S2). Note that all
79 measurements were performed at 28 °C where the growth rate is expected to be about 2 times slower
80 than at 37°C [31]. Using the fluorescently labeled strain we followed the timing of replication termination
81 (T_{rt}), onset of FtsN accumulation at mid-cell (T_n) and onset of constriction (T_c) in time-lapse images (Fig.
82 1A-B). Here all the times are given relative to cell birth. Additionally, we also determined the timing of
83 replication initiation (T_{ri}) and the C-period ($C = T_{rt} - T_{ri}$). We determined T_{ri} , T_{rt} and T_n from the
84 analysis of fluorescent images and T_c from the phase images (for details see Methods). We found T_c to

85 be delayed relative to T_n on average by about 12 mins (SI Fig. S1). We assign the delay to less sensitive
86 determination of constriction formation from phase images. We therefore use T_n instead of T_c for the
87 timing of the constriction formation in the Figures in the main text while the data on T_c can be found in
88 SI Figures.

89 We first investigated the correlation between termination and onset of constriction times in slow growth
90 conditions in the M9 glycerol medium (Fig. 1C). The T_n and T_{rt} times were correlated (with a Pearson
91 correlation coefficient $R = 0.94$) as were also T_c and T_{rt} times ($R = 0.92$; SI Fig. S1). The comparable
92 timings and correlations between T_c and T_{rt} time were also present in a different strain which carried
93 *ssb*-Ypet label for replisome and no divisome label (Fig. S2) indicating that Ypet fusion to FtsN and mCherry
94 fusion to DnaN did not have significant effects on division and replication processes.

95 In 7% of cells, we found the onset of constriction as measured by Ypet-FtsN (i.e., T_n) occurred before the
96 termination (T_{rt}) (Fig. 1D). When we determined the onset of constriction from the phase images (T_c),
97 in only 1 out of 420 cells termination occurred earlier than the onset of constriction (SI Fig. S1) but as
98 argued earlier the latter estimate is likely less accurate. For 7% of cells, in which the initiation of
99 constriction preceded the termination, the distribution of times $T_n - T_{rt}$ was approximately exponential
100 with a characteristic time of 7 min (inset of Fig. 1D). The latter time is close to the characteristic time that
101 DnaN remains attached to the replication terminus region after completion of replication (3 mins at 37
102 °C, potentially translating to about 6 mins in our conditions) [25]. Altogether, the fraction of cells in which
103 the termination of replication occurs after the *actual* onset of constriction is much smaller than 7%, if not
104 zero. Interestingly, the distribution of $T_n - T_{rt}$ was also approximately exponential for positive values
105 with a characteristic time of 15 mins (Fig. 1D, inset). The latter suggests the possibility of a single rate-
106 limiting reaction associated with the process of triggering constriction formation that follows the
107 termination, as we elaborate on later.

108 We next investigated how the above conclusions applied at different growth rates. We repeated these
109 measurements in eight additional different growth media (SI Table S3); in three of these, the growth rates
110 were slower while in the other five the rates were higher than in the measurement discussed above (SI
111 Table S2). In all of these nine growth conditions, the average delay time $\langle T_n - T_{rt} \rangle$ was positive showing
112 that constriction formation follows on average the termination and possibly in all divisions (Fig. 2A, inset).
113 $\langle T_n - T_{rt} \rangle$ showed variation between 20 min to 40 mins in different growth rates except for the slowest
114 growth rate in acetate medium where $\langle T_n - T_{rt} \rangle \approx 65 \text{ min}$. Unlike the almost growth rate-independent
115 behavior of $\langle T_n - T_{rt} \rangle$, the normalized delay times, $\langle (T_n - T_{rt})/T_d \rangle$, showed two distinct growth-rate
116 dependent regimes (Fig. 2A). Below about $T_d \approx 130 \text{ mins}$ the normalized times decreased as the
117 doubling time increased but above it, the values plateaued reaching about 12% of the cell cycle. A similar
118 cross-over from one regime to another was also seen in Pearson correlation coefficients, $R(T_n, T_{rt})$ (Fig.
119 2B). For $T_d > 130 \text{ mins}$ the termination of replication and the onset of constriction were highly
120 correlated ($R(T_n, T_{rt}) > 0.85$) and independent of T_d , while for $T_d < 130 \text{ mins}$ these correlations
121 decreased approximately linearly with the decreasing T_d . A similar cross-over behavior could be also seen
122 in plots when the timing of constriction (T_c) was determined from phase images (SI Fig. S3).

123 The times of termination and constriction initiation were not only correlated but furthermore followed a
124 timer-like relationship, $T_n = T_{rt} + \text{constant}$, at slower growth rates. This was evident in plots of T_{rt} vs
125 T_n where linear regression gave a slope of ≈ 1 for longer doubling times (Fig. 2C). The corresponding
126 intercept of the fits was almost independent of the doubling time (SI Fig. S4A). We also found that the
127 distribution of delay times $T_n - T_{rt}$ in a given growth condition was approximately exponential at slower
128 growth rates, as it was for the growth condition described above (SI Fig. S4B). This was also reflected in
129 the coefficient of variation (CV) of these distributions, which was approximately one at longer doubling
130 times (Fig. 2D). The CV values also showed a cross-over at $T_d \approx 130 \text{ mins}$. In shorter doubling times, the
131 CV values decreased and the mode of the $T_n - T_{rt}$ distributions shifted to positive values (SI Fig. S4B).

132 Altogether, the exponential distribution of delay times and the timer behavior in a range of slow growth
133 conditions suggest a constant rate process linking onset of constriction to replication. The process may
134 result from a single first-order reaction with some rate-limiting component. Irrespective of the details of
135 this process, for $Td > 130$ mins our data is consistent with the idea that some replication related process
136 controls the initiation of constriction but as the doubling times shorten this process becomes less and less
137 rate-limiting.

138 **Model supports checkpoint for constriction to be close to termination in slow growth conditions**

139 The presented data in slow growth conditions suggest that there is a replication-dependent checkpoint
140 for the onset of constriction. However, it may occur before the termination of replication. To narrow down
141 the possible time range for this checkpoint we constructed an analytical model. The model allows us to
142 calculate the $Tn - Trt$ distributions and various statistics related to the processes as a function of the
143 timing of the checkpoint, Tx (Fig. 3A). In the following discussion, we define the normalized time
144 difference $x = (Trt' - Tx)/\langle C \rangle$, namely the time delay between the true termination event, Trt' (as
145 opposed to the *measured* termination event Trt) and the checkpoint Tx . In the above expression $\langle C \rangle$ is
146 the average C-period in a given growth condition. x ranges from 0 to 1, with $x = 0$ corresponding to a
147 checkpoint at the termination and $x = 1$ to one at the initiation of replication. We furthermore assume
148 that when the replication fork reaches a relative distance x from the replication terminus, initiation of
149 constriction occurs with a constant rate r (i.e., consistent with first-order reaction kinetics). The
150 assumption of a single rate constant is based on the approximately exponential distribution for $Tn - Trt$
151 (for positive values) (Fig. 1D, SI Fig. S4B) as well as the CV of this distribution being approximately equal
152 to 1 (Fig. 2E) in slow growth conditions. The model also accounts for the difference between the measured
153 value of Trt and the actual one (Trt') due to the finite time DnaN remains DNA bound after replication
154 completes. The attachment time of DnaN has been found to be exponentially distributed [25]. As
155 discussed previously, a mean time of $\langle Ta \rangle = 3$ to 6 mins can be expected in our growth conditions.

156 Under these assumptions, we find that the CV of the $Tn - Trt$ distribution is given by:

$$157 \quad CV(Tn - Trt) = \frac{\sqrt{\left(\frac{1}{r}\right)^2 + \sigma_C^2 x^2 + \langle Ta \rangle^2}}{\frac{1}{r} - \langle C \rangle x - \langle Ta \rangle}, \quad (1)$$

158 (see Model in Methods for the derivation). Here, σ_C is the standard deviation for the distribution of C-
159 periods within the cell population. All the quantities except x in eq. 1 (namely $\langle C \rangle$, σ_C , r , $\langle Ta \rangle$) are
160 determined from experiments (see Model in Methods). We compared the predictions of the above
161 formula to the measured CV values in the four slowest growth conditions. Eq. 1 predicts that
162 $CV(Tn - Trt)$ is close to 1 near $x = 0$ and rises rapidly with increasing x for all growth conditions
163 considered (Fig. 3B). The experimentally measured CV values are thus consistent with the model only
164 when x is close to zero, that is when the constriction is initiated shortly before or at termination.

165 The Pearson correlation coefficients between Tn and Trt (Fig. 3C) and the slopes of Tn vs Trt linear fits
166 (Fig. 3D), both of which can be derived analytically within the model, also show an agreement with the
167 experimental data only when x is close to zero. In some growth conditions, however, the best agreement
168 between model and data for the slope of Tn vs Trt occurs for larger values of x . The most outlying point
169 in Fig. 3D corresponds to mannose where the data and the model agree at $x = 0.2$. Nonetheless, most
170 data appear to be consistent with the checkpoint at the termination. Indeed, taking $x = 0$, we could
171 explain satisfactorily the entire distribution of $Tn - Trt$ for all slow growth conditions (Fig. 3E).

172 To further test the model, we also compared correlations and statistics between experimentally
173 determined replication initiation, Tri and constriction initiation, Tn , timings (SI Fig S5 A-D, Table S4). We
174 found that the model agrees with the experimental values of $CV(Tn - Tri)$ and $R(Tri, Tn)$ in all slow
175 growth conditions for $x < 0.2$ (SI Fig. S5 E-F). In particular, the model predicts the slope of Tn vs Tri to
176 be exactly one for all values of x , which is indeed observed experimentally (SI Fig. S5C). Altogether, the
177 data and the model can be reconciled for the whole dataset if one assumes that the checkpoint is no more

178 than $0.2C$ from the termination but most likely at the termination. It is important to emphasize that the
179 agreement between the data and model can only be achieved for slow growth conditions ($Td >$
180 130 mins). For faster growth rates the model and the data do not agree for any values of x . This
181 disagreement can be expected because the model assumes some replication-related process leading to
182 onset of constriction. As argued above, this assumption is not likely valid at faster growth rates.

183 **Constriction can start before replication termination if the divisome is misplaced**

184 Our goal was then to elucidate the molecular mechanism(s) that could be responsible for triggering
185 constriction formation in a replication-dependent manner. Several molecular systems have been
186 identified in the past that couple division and replication cycles in *E. coli* [32]. These include the nucleoid
187 occlusion factor SlmA [33], the Ter linkage proteins ZapA, ZapB, and MatP [34, 35], and the DNA
188 translocase FtsK [36]. The first two of these systems have been implicated in the positioning of the Z-ring
189 relative to the replication terminus region of the chromosome while FtsK can reposition misplaced
190 chromosomes relative to the division plane at the end of constriction [37]. We next asked if any of these
191 systems are responsible for the correlated timing between the termination of replication and initiation of
192 the constriction. We first considered the effects of SlmA, which is proposed to inhibit the formation of the
193 Z-ring before the Ter region of the chromosome moves to the center of the cell in a replication-dependent
194 manner [32, 38]. Its inhibitory effect is believed to be relieved from the mid-cell in the 2nd half of the
195 replication period because SlmA lacks binding sites at the Ter region. By removing SlmA from the cell one
196 would expect the formation of the Z-ring and the constriction to start earlier. In contrast to this prediction,
197 our data show that the $Tn - Trt$ period increased compared to the WT strain in slow growth conditions
198 ($p = 4 \cdot 10^{-4}$; in single tailed Mann-Whitney test, Fig. 4A & Table S5). At the same time $R(Tn, Trt)$
199 decreased compared to WT but still remained present at a significant level ($R = 0.7$; Fig. 4B). The
200 observations clearly rule out the idea that SlmA is the main factor responsible for the timing of constriction

201 formation. Rather, the above findings indicate that SlmA affects the timing of constriction indirectly by
202 modulating the activity of some other factor.

203 Next, we investigated the role of the Ter linkage proteins ZapA, ZapB, and MatP. Unlike SlmA, which acts
204 as an inhibitor, these proteins have been implicated in promoting the formation of the Z-ring [35].
205 Together ZapA, ZapB, and MatP form a proteinaceous chain that connects the replication terminus region
206 of the chromosome to the Z-ring. For this connection, all three proteins are needed [34]. Since these
207 proteins promote Z-ring formation, removal of either ZapA, ZapB, or MatP from cells should delay Z-ring
208 formation and possibly also the formation of the constriction. Indeed, removal of either of these three
209 proteins increased $\langle T_n - T_{rt} \rangle$ in a statistically significant manner (SI Table S5) although the magnitude
210 of the effect was small (less than 10% of cell cycle time; < 15 mins). The observed small increase in delay
211 in constriction formation indicates that the Ter linkage proteins, similarly to SlmA, are unlikely to be
212 directly involved in timing the constriction formation.

213 We also investigated the role of FtsK. FtsK has been implicated in segregating the replication terminus
214 region at the onset of constriction [39, 40]. One could expect the unsegregated terminus region to delay
215 constriction closure. Using a translocation defective mutant FtsK K997A [41] we indeed found
216 $\langle T_n - T_{rt} \rangle$ time to increase but the observed effect was again rather small (11 min; 7% of cell cycle time).
217 Thus, all these mutants showed increased $\langle T_n - T_{rt} \rangle$ periods compared to WT cells and slightly lower
218 correlations in $R(T_n, T_{rt})$ (Fig. 4B) but these effects were small enough to rule out their direct
219 involvement in triggering the constriction formation. The observed small effects of these deletions arise
220 likely via small changes these proteins have on the structure and composition of the divisome, and on the
221 organization of the chromosome.

222 Although the Min system is not known to directly couple the replication and division processes, it is one
223 of the main determinants for positioning the Z-ring in *E. coli* [32]. In cells with a defective Min system, a

224 fraction of divisions occurs close to cell poles while the remaining ones still occur in the vicinity of cell
225 middle. Distinguishing polar divisions from mid-cell ones shows that polar divisions can start significantly
226 earlier than the mid-cell ones (Fig. 4C, D). About half of the polar divisions started before replication had
227 terminated. At the same time, the timing of mid-cell divisions was not affected compared to WT cells
228 (inset of Fig. 4D). The findings related to polar divisions rule out the possibility that termination *triggers*
229 constriction formation as such a trigger would violate causality. On the other hand, these data raise the
230 possibility that replicating nucleoids in mid-cell can block constriction formation. According to the
231 previous discussion, this blockage is not dependent on the nucleoid occlusion factor SlmA.

232 **Discussion**

233 We found that the initiation of the constriction and the termination of the replication in *E. coli* were poorly
234 correlated at fast growth rates but the correlations increased as the growth rate slowed reaching $R =$
235 0.94 for the slowest growth condition. The cross-over from a correlated to uncorrelated regime occurred
236 approximately at $Td \approx 130$ mins, which corresponds to $Td \approx 65$ mins at 37°C . A similar cross-over also
237 appeared in $CV(Tn - Trt)$ and in the slope of Trt vs Tn when plotted against Td . Furthermore, the
238 distributions of delay times $Tn - Trt$ become approximately exponential for $Td > 130$ mins suggesting
239 that the replication is rate-limiting for the initiation of constriction.

240 One of our aims was to further elaborate on the coupling mechanism between replication and division
241 cycles. The measurements with the *minC* deletion strain in slow growth conditions showed that in polar
242 divisions initiation of constriction can precede termination of replication while the mid-cell divisions
243 followed the same timings as in WT cells. This finding ruled out the possibility that termination acts as a
244 trigger for constriction formation. Also, the finding ruled out that there can be a diffusible signal that
245 triggers constriction formation which is released at [42] or before termination. The diffusible signal should
246 reach within seconds all cellular locations including mid cell and pole, and it will not lead to observable

247 differences in the timing of constriction formation. Note that a protein synthesized in response to
248 transcriptional activation is a diffusible signal. The data thus rule out any possible mechanism where
249 initiation of constriction is triggered in response to transcriptional activation of some gene. Instead of
250 being triggered, the data from polar divisions suggested that a replicating and not fully segregated
251 chromosome in the mid-cell blocks constriction formation; that is, replication related processes license
252 the onset of constriction.

253 Although the coupling between the replication and division cycles appears to involve some form of
254 nucleoid occlusion, it appears not directly related to the nucleoid occlusion factor SlmA. Clearly, there
255 could be some unknown nucleoid occlusion factor that is not identified yet as argued before [35, 43, 44].
256 It is also possible that there are no additional proteins involved but the nucleoid occlusion arises directly
257 from chromosome coils or transesterion linkages [32], which present a steric hindrance for the formation
258 and maturation of the Z-ring. These possibilities should be examined in further studies.

259 Altogether, our data indicate that there is a mechanism to license division in a replication-dependent
260 manner (Fig. 5). In slow growth conditions, this licensing is rate-limiting for constriction formation. Our
261 modeling studies suggest that the replication-dependent checkpoint occurs most likely at the termination
262 but not earlier than $0.2C$ from the termination. Once the division is licensed, the constriction formation
263 ensues via reaction kinetics which is suggestive of first-order reaction. At faster growth rates some other
264 competing process appears to become rate-limiting. The origin of the “other” process remains to be also
265 determined. Some authors have proposed the rate-limiting factors for the onset of constriction are
266 precursor molecules for peptidoglycan synthesis [10] such as lipid II while others have concluded that it is
267 the protein FtsZ [8]. Further work is thus needed to clarify the origin of this process.

268 The regulation proposed in Fig. 5 is similar to the concurrent processes model [11, 12] with some
269 differences. First, the concurrent processes model does not consider the initiation of the constriction as a

270 cell cycle checkpoint. Instead, it predicts the timing and cell size at the division; that is at the end of all
271 division-related processes. Note that all other current cell cycle models in *E. coli* also predict only the end
272 of the division. Second, in the concurrent processes model replication and growth-related processes are
273 both rate-limiting for division in all growth conditions. Our data suggest that replication is rate-limiting for
274 constriction only in slow growth conditions and the concurrency of the processes is only significant at the
275 vicinity of the cross-over region.

276 In conclusion, our work has shown that cell division is limited by replication-related processes in slow
277 growth conditions but appears to be almost independent of these processes in fast growth. This behavior
278 might explain why some earlier works have inferred that replication and division cycles are completely
279 uncoupled from each other [8-10] while other authors have come to exactly opposite conclusions [1, 2, 6,
280 7]. Our data furthermore implies that the limitation related to replication processes stems from some yet
281 to be identified form of nucleoid occlusion. This nucleoid occlusion is lifted in a replication-dependent
282 manner. In parallel to this limitation, cells experience other types of licensing conditions that need to be
283 met. Whether all these limiting processes couple to the divisome via the central hub of FtsZ protofilaments
284 or also via other divisome components remains to be elucidated.

285

286 **Acknowledgments**

287 The authors thank Ethan Garner, Conrad Woldringh and Arie Zaritsky for useful discussions, Da Yang and
288 Scott Retterer for help in microfluidic chip making. Authors acknowledge technical assistance and material
289 support from the Center for Environmental Biotechnology at the University of Tennessee. A part of this
290 research was conducted at the Center for Nanophase Materials Sciences, which is sponsored at Oak Ridge
291 National Laboratory by the Scientific User Facilities Division, Office of Basic Energy Sciences, U.S.
292 Department of Energy. This work has been supported by the US-Israel BSF research grant 2017004 (JM),

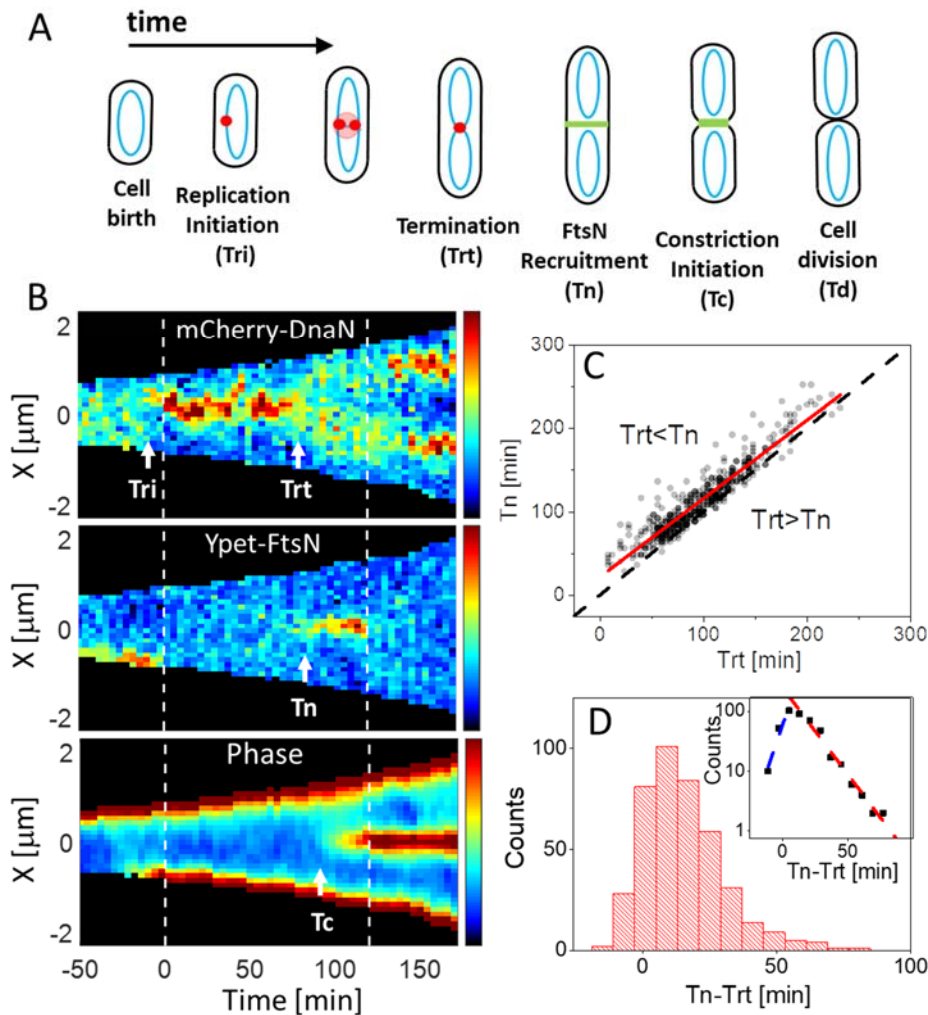
293 the National Institutes of Health award under R01GM127413 (JM), NSF CAREER 1752024 (AA) and NSF
294 award 1806818 (PK).

295

296 **Conflict of interest**

297 The authors declare that they have no conflicts of interest with the contents of this article.

Figures



298

299 **Figure 1. Timing of constriction formation and recruitment of FtsN relative to termination of replication**

300 **in slow growth conditions.** (A) Schematics for the main cell cycle events and timings that are determined

301 from time-lapse measurements. (B) Kymographs of fluorescent and phase signals for a representative cell

302 grown in M9 glycerol medium. Dashed vertical lines indicate cell division events. Red corresponds to high

303 and blue to low-intensity values. Event timings are indicated by arrows. (C) Termination of replication

304 (T_{rt}) vs initiation of constriction (T_n) for a population of cells ($N=420$). T_n is determined based on the

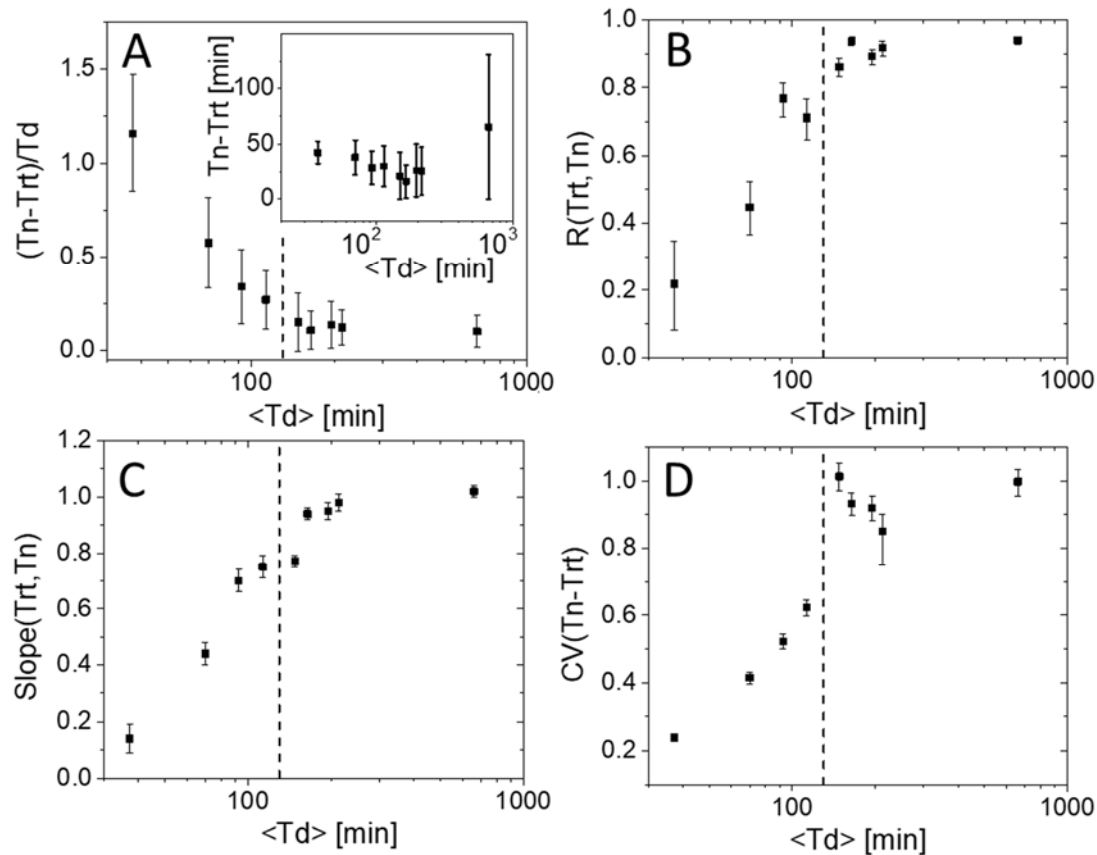
305 accumulation of Ypet-FtsN signal at mid-cell. The solid red line is a linear fit with ($T_n = 0.94T_{rt} +$

306 22 mins). The dashed black line corresponds to $T_{rt} = T_n$. (D) Distribution of delay times between

307 constriction formation and termination of replication for these cells. Inset shows the same data in a semi-

308 logarithmic plot. The dashed lines are fits to exponential decay. The time constant for the fit at negative

309 times is 7 min and for positive times 15 mins.



310

311 **Figure 2. Comparison of timings of constriction initiation and termination of replication in 9 different**

312 **growth media.** From the longest to shortest doubling times the carbon sources used in the media are

313 acetate, alanine, mannose, glycerol, glycerol + trace elements (TrEI), glucose, glycerol+Cas, glucose+Cas,

314 and EZ-Rich defined medium with glucose (for details see Table S3). (A) The average normalized delay

315 time between initiation of constriction and termination of replication as a function of the average

316 doubling time, $\langle Td \rangle$. Inset shows the unnormalized CV delay time. Error bars in both plots show the std of

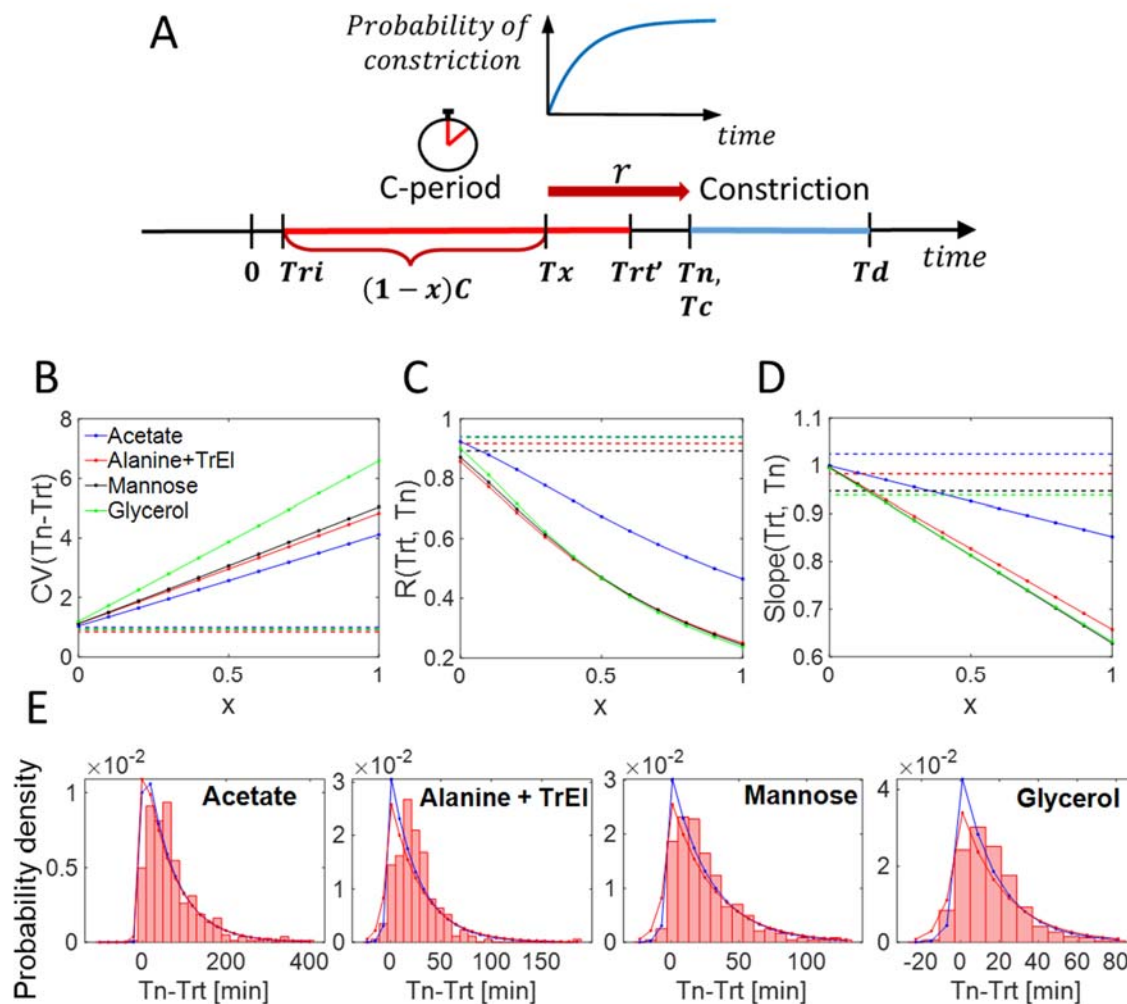
317 these quantities within the cell population. (B) Pearson correlation coefficient between Trt and Tn . (C)

318 The slope of Trt vs Tn plot. (D) Coefficient of variation for $Trt - Tn$ distribution. The dashed vertical lines

319 in all plots correspond to $\langle Td \rangle = 130$ min. Error bars in (C)-(F) show 95% confidence intervals. For

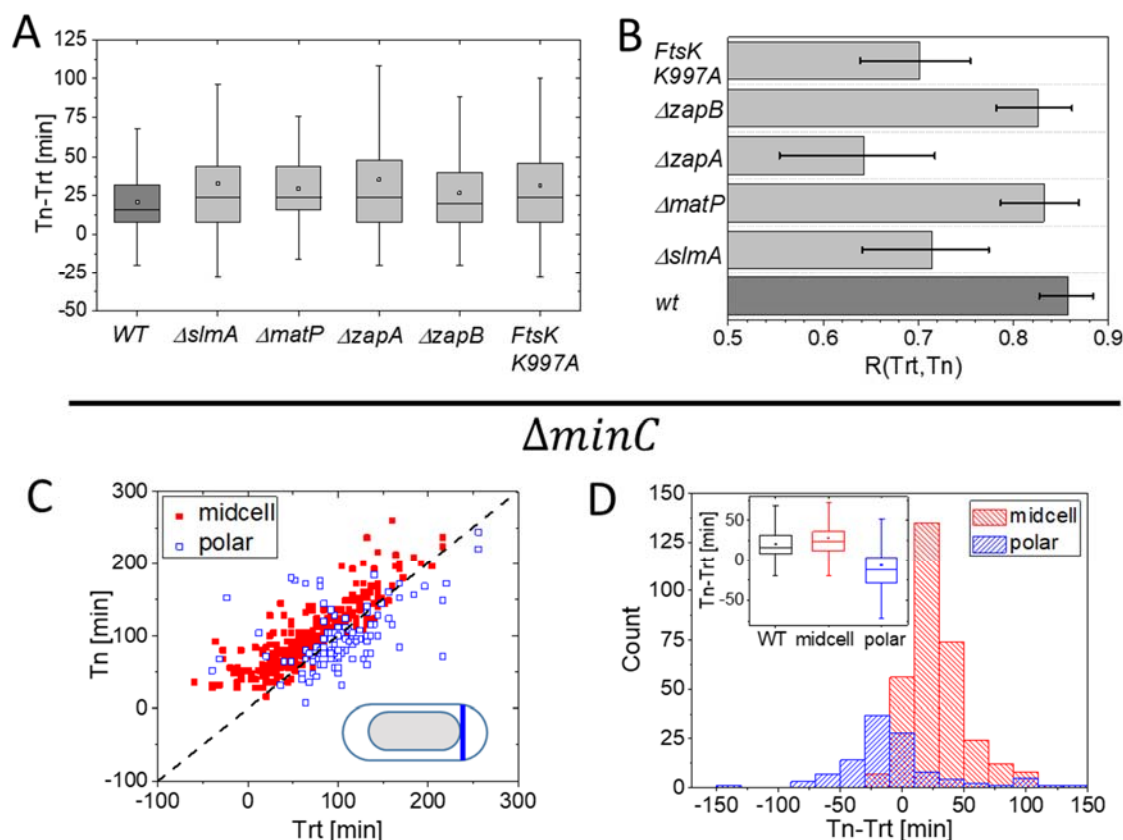
320 calculation of these intervals see Methods.

321



322
 323 **Figure 3: Predictions of model coupling the replication cycle to the onset of constriction.** (A) Schematics
 324 representing the model. T_x is the timing for the checkpoint that triggers constriction formation. x is the
 325 normalized time of this checkpoint from termination. Trt' is the actual time of termination, which differs
 326 from the measured time Trt by the detachment time of mCherry-DnaN from the chromosome (see
 327 Methods for details). (B) Coefficient of variation of the $T_n - Trt$ distribution, (C) Pearson correlation
 328 coefficient between Trt and T_n , and (D) the slope of the linear regression line for T_n vs Trt all plotted as
 329 a function of x . In panels (B)-(D) the solid lines show predictions of the model and the dashed horizontal
 330 lines the experimental values. Note that only the four slowest growth conditions are considered in these
 331 comparisons and $\langle Ta \rangle = 3$ min. (E) Distribution of $T_n - Trt$ for slow-growth conditions obtained from
 332 experiments and from theory for two different values of $\langle Ta \rangle$. The theoretical distributions are given by
 333 eq. 20 in Methods and they correspond to $x = 0$. Blue lines correspond to $\langle Ta \rangle = 3$ min, and red lines to
 334 $\langle Ta \rangle = 6$ min. All other parameters in eq. 20 are determined from the data.

335

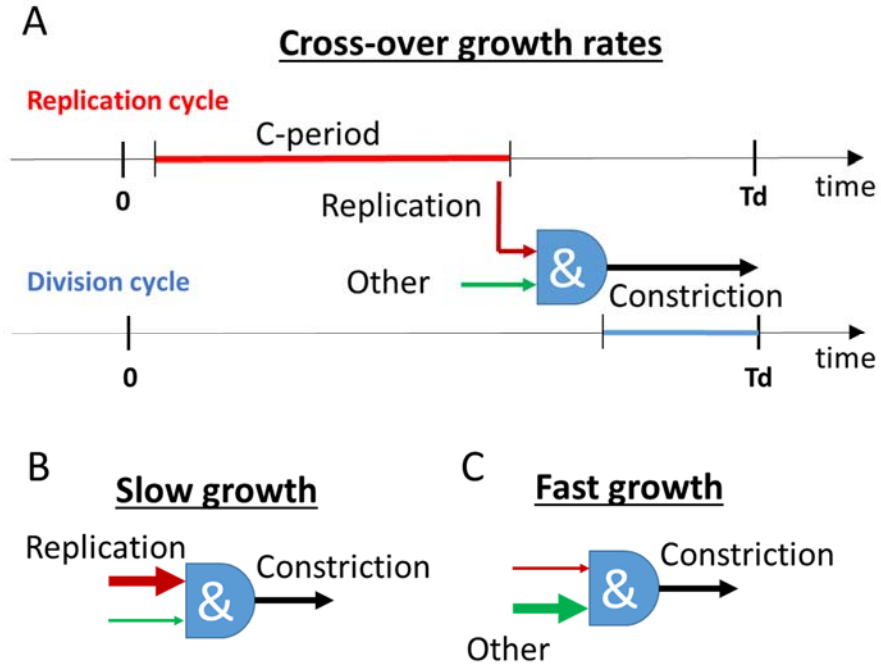


336

337

338 **Figure 4. Timings for termination of replication and constriction initiation for different deletion**
 339 **mutants.** The deleted gene products have been implicated in coordinating division and replication
 340 processes. (A) Delay times between the termination and initiation of constriction for wildtype (WT),
 341 $\Delta slmA$, $\Delta matP$, $\Delta zapA$, $\Delta zapB$, and $ftsK$ K997A strains. All mutant strains show longer delay times
 342 compared to WT strain at $p = 0.05$ level except $\Delta zapA$ (Mann-Whitney test; Table S5). (B) Pearson
 343 correlation coefficients between these times for the same strains. Error bars reflect 95% confidence
 344 intervals. (C) Termination of replication (Trt) vs initiation of constriction (Tn) for $\Delta minC$ cells. Polar
 345 divisions and mid-cell divisions are separately labeled. (D) Distribution of corresponding delay times in this
 346 strain. Inset compares the distributions to the corresponding one in WT cells. All measurements were
 347 performed in M9 Gly+TrEI medium.

348



349

350 **Figure 5. Regulation of constriction formation in different growth rates.** (A) Regulation at the cross-over
351 regime where $Td \approx 130 \text{ min}$. The corresponding doubling times at 37°C are expected to be about twice
352 shorter. The replication period is shown by red and the constriction period by blue lines. & sign indicates
353 an integration of different signals. Constriction starts when conditions imposed by the replication and by
354 some “other” yet to be identified processes have been both met. Replication related processes relieve
355 inhibition for initiation of constriction at or shortly before the termination. (B) In slow growth conditions,
356 the onset of constriction is rate-limited by replication-related processes. (C) In fast growth conditions,
357 some unknown “other” process(es) become rate-limiting.

STAR METHODS

KEY RESOURCES TABLE

| REAGENT or RESOURCE | SOURCE | IDENTIFIER |
|--|---|-----------------|
| Bacterial Strains | | |
| SeeTable S1a | | |
| Chemicals, Peptides, and Recombinant Proteins | | |
| Chloramphenicol | <i>MilliporeSigma</i> | Cat#C0378-5G |
| Kanamycin | <i>MilliporeSigma</i> | Cat#K4000-5G |
| Ampicillin | <i>MilliporeSigma</i> | Cat#A0166-5G |
| Glucose | <i>MilliporeSigma</i> | Cat#G8270-100G |
| Glycerol | <i>Fisher BioReagents</i> | Cat#BP229-1 |
| Alanine | <i>Fisher BioReagents</i> | Cat#BP369-100 |
| Mannose | <i>MilliporeSigma</i> | Cat#M6020-25G |
| Sodium acetate (acetate) | <i>MilliporeSigma</i> | Cat#S5636-250G |
| Thymine | MP Biomedicals | Cat#0210306025 |
| Casamino acids (Cas) | ACROS Organics | Cat#AC612041000 |
| Isopropanol | Fisher Chemical | Cat#A464-4 |
| Bovine Serum Albumin (BSA) | <i>MilliporeSigma</i> | Cat#A7906-10G |
| M9 minimal media | Teknova.com | Cat#M1902 |
| EZ Rich Defined Medium (EZRDMD) | Teknova.com | Cat#M2105 |
| Trace metal elements mixture | Teknova.com | Cat#T1001 |
| Sylgard 184 | Dow Corning | N/A |
| Oligonucleotides | | |
| SeeTable S1b | | |
| Software and Algorithms | | |
| MATLAB R2017a | Mathworks, Inc | RRID:SCR_001622 |
| NIS-Elements | Nikon Instruments Inc. | RRID:SCR_014329 |
| DiplImage toolboxes | http://www.diplib.org/ | |
| Python 3.7 | https://www.python.org | RRID:SCR_008394 |
| Other | | |
| Nikon Ti-E inverted microscope | Nikon Instruments Inc. | Cat# MEA53100 |
| Nikon Perfect Focus system | Nikon Instruments Inc. | Cat# MEP59390 |
| Andor EMCCD camera | Oxford Instruments | iXon897 |
| O ₂ plasma asher | March Instruments | Plasmod |
| Syringe pump | New Era Pump Systems | Model: NE-1000 |
| Syringe pump | New Era Pump Systems | Model: NE-2000 |

CONTACT FOR REAGENT AND RESOURCE SHARING

Further information and requests for resources and reagents should be directed to and will be fulfilled by the Lead Contact, Jaan Männik (JMannik@utk.edu).

358 **METHODS**

359

360 **Construction of *E. coli* strains**

361 All *E. coli* strains used in the reported experiments are derivatives of K12 BW27783 obtained from the
362 Yale Coli Genetic Stock Center (CGSC#: 12119). Strains were constructed either by λ -Red engineering [45]
363 and/or by P1 transduction. Where necessary kanamycin resistance gene was removed by expressing the
364 Flp recombinase from plasmid pCP20 [46]. Detailed information of strain genotypes and construction
365 information is listed in Table S1a. Oligonucleotide information is given in Table S1b. For *E. coli* strain
366 engineering, cells were grown in lysogeny broth (LB) and appropriate selective antibiotics.

367

368 **Growth media and growth conditions**

369 For time-lapse imaging in microfluidic devices, cells were cultured in 9 different growth conditions at 28°C.
370 Detailed information on the media used can be found in SI Table S3.

371

372 **Cell preparation and culture in microfluidic devices**

373 All bacterial strains were streaked on agar plates containing M9 minimal salts supplemented with 2 mM
374 magnesium sulfate, corresponding carbon sources, and appropriate selective antibiotics. A day before an
375 experiment a less than 10 days old colony was inoculated into 3 ml of EZ Rich Defined Medium (EZRD, M,
376 Teknova Inc., CA) or M9 minimal salts media (Teknova Inc., CA) supplemented with corresponding carbon
377 sources, trace metals mixture (Teknova Inc., CA, #T1001), casamino acids (ACROS Organics) and
378 appropriate antibiotics when needed. Unless otherwise indicated, antibiotics were used at 25 μ g/ml of
379 kanamycin (Kan) and 25 μ g/ml chloramphenicol (CM). For microscopy experiments, cells were grown to
380 an OD₆₀₀ of ~0.1 in a liquid medium and then concentrated ~100x by centrifugation in presence of 0.75
381 μ g/ml of BSA (Bovine Serum Albumin; Millipore Sigma, MO) to minimize clumping of the cells. The
382 resulting solution was used to inoculate microfluidic mother machine devices. The latter were made of
383 PDMS (polydimethylsiloxane) following a previously described procedure [30]. For inoculation 2-3 μ l of
384 resuspended concentrated culture was pipetted into the main flow channel of the device. The cells were
385 then let to populate the dead-end channels. Once these channels were sufficiently populated (about 1
386 hr), tubing was connected to the device, and the flow of fresh M9 medium with corresponding carbon
387 sources and supplements, and BSA (0.75 μ g/ml) was started. The flow was maintained by a NE-1000
388 Syringe Pump (New Era Pump Systems, NY) at 5 μ l/min during the entire experiment. To ensure steady-

389 state growth, the cells were left to grow in channels at least 14 hr (24 hrs for acetate) before imaging
390 started.

391

392 **Fluorescence microscopy**

393 A Nikon Ti-E inverted fluorescence microscope (Nikon Instruments, Japan) with a 100X NA 1.40 oil
394 immersion phase contrast objective (Nikon Instruments, Japan), was used for imaging the bacteria. Images
395 were captured on an iXon DU897 EMCCD camera (Andor Technology, Ireland) and recorded using NIS-
396 Elements software (Nikon Instruments, Japan). Fluorophores were excited by a 200W Hg lamp through an
397 ND4 and ND8 neutral density filter. Chroma 41004 and 41001 filter cubes (Chroma Technology Corp., VT)
398 were used to record mCherry and Ypet images, respectively. A motorized stage (Prior Scientific Inc., MA)
399 and a Nikon Perfect Focus[®] system were utilized throughout time-lapse imaging.

400

401 **Image analysis**

402 MATLAB, along with the Image Analysis Toolbox and Diplib Image Toolbox, (<http://www.diplib.org/>) were
403 used for image analysis. In all analyses of time-lapse recordings, corrections to subpixel shifts between
404 different frames were applied first. These shifts were determined by correlating phase-contrast images in
405 adjacent frames. The cells were then segmented based on phase-contrast images using a custom MATLAB
406 script. The segmented images were used to compile heatmaps of phase and fluorescent images as shown
407 in Fig. 1B. Timings of cell divisions were corrected based on the dissociation of the Ypet-FtsN label from
408 the septum in strains where this label was present. Timings of replication initiation and termination, and
409 initiation of constriction were determined from heatmaps. For the Figures in the main text the replication
410 initiation, T_{ri} , and termination, T_{rt} , timings were determined from the heatmaps of the mCherry-DnaN
411 label (strain STK13). For a detailed procedure see below. In glycerol and glucose+Cas growth media, these
412 timings were also determined using a different strain (JM85), which expressed the ssb-Ypet label. The
413 data from the latter strain are shown in SI Figures. Timings for the onset of FtsN recruitment to the Z-ring,
414 T_n , were determined from Ypet-FtsN heatmaps. The onset of constriction, T_c , was determined from
415 phase heatmaps for both strains.

416

417 **Determination of T_{rt} timing**

418 In slow growth conditions, there is typically a single termination that increases the number of
419 chromosomes from one to two while at faster growth rates a fraction of cells is born with two
420 chromosomes. To analyze cells born with one and two chromosomes on the same footing we considered

421 the relevant termination for the cells born with two chromosomes to occur in the mother cell. Using this
422 analysis, the termination times of the cell population have a continuous unimodal rather than bimodal
423 distribution. In this distribution, the times of replication termination are negative if these times occur in
424 the mother cell. The two terminations in the mother cell were not exactly synchronous. For a given cell of
425 interest, we determined the timing of the termination for the chromosome that was inherited by this cell.
426

427 **Determination of *Trt* timing**

428 Similar to the termination, the relevant initiations of replication could occur in the mother cell. In the two
429 fastest growth rates, in EZ-Rich and M9 glucose+CAS the relevant initiations could also occur in the
430 grandmother cells. Our analysis routine did not allow us to determine these events. Also, in these two
431 growth conditions even when the initiations occurred in the mother cell it was rather ambiguous to
432 determine their timing. We, therefore, left out these two growth conditions from the analysis that
433 involved replication initiation (in SI Fig. S5 and Table S4). The timing of replication termination (*Trt*) could
434 still be reliably determined in these conditions. In other growth media, the initiation occurred either in
435 the mother cell or in the cell of interest. If the initiation occurred in the mother cell then the timing of the
436 initiation of the chromosome that was inherited by the cell of interest was used. The time difference
437 between the two initiations in the mother cell was typically within 8 min interval.
438

439 **Statistical Analysis/Error Analysis**

440 Different distributions of $Tn - Trt$ times were compared using t-test and Mann-Whitney test. For testing
441 Matlab functions *ttest2* and *ranksum* were used, respectively.
442

443 Error bars for the Pearson R-values represent 95% confidence intervals. These intervals were calculated
444 using Fisher's z-transformation [47]. Briefly, based on the measured R-value corresponding z-value was
445 calculated as $z = 1/2 \ln(1 + R/1 - R)$. The 95% confidence intervals for z were calculated as $z_{CI} = [z -$
446 $1.96/\sqrt{N - 3}, z + 1.96/\sqrt{N - 3}]$ where N is number of measurements for a given R-value. The intervals
447 were then backtransformed for R confidence intervals using $R_{CI} = (\exp(2z_{CI}) - 1)/(\exp(2z_{CI}) + 1)$.
448

449 Error bars for the coefficient of variation (CV) also represent 95% confidence intervals. These intervals
450 were determined by bootstrapping. Bootstrapping was carried out in Phyton 3.7. by sampling the
451 distributions 10^4 times and verifying that the resulting CV distributions did not change upon further
452 doubling the samples. Percentile intervals were found using *numpy percentile* method.

453

454 **Model coupling replication and constriction**

455 We assume that cells initiate DNA replication at time Tri and that nucleotides are added to the growing
456 strand of DNA at a constant rate γ . We denote the length of the *E. coli* genome (measured in nucleotide
457 number) as N . Using the central limit theorem, the time taken to reach termination (the C period) is
458 normally distributed with a mean $\frac{N}{\gamma}$ and variance $\frac{N}{\gamma^2}$. The CV of the C period thus scales as $\frac{1}{\sqrt{N}}$ with $N \approx$
459 $4 \cdot 10^6$. Thus, the predicted CV is two orders of magnitude smaller than that experimentally observed (SI
460 Table S4), and we conclude that the variability in the C period resulting from stochastic nucleotide
461 addition is negligible. Hence, we can consider the replication process to be happening at a constant
462 velocity v . The time taken for replication to complete is then given by $\frac{N}{v}$, and variability in the C period
463 results from the cell-to-cell variability in v .

464 Experimentally, the C period and Td are strongly and positively correlated (SI Table S4). This would
465 suggest that the progress of biochemical processes like DNA replication scales with the individual growth
466 rate of the cells. In this case, a slower-growing cell will also replicate at a slower velocity and subsequently
467 have a longer C period. The scaling with growth rate points to a small but non-negligible variability in v
468 within the population of growing cells in a particular media.

469 Since C is assumed uncorrelated with the initiation time, the time at termination Trt' is thus:

$$470 \quad Trt' = Tri + C. \quad (1)$$

471 The evidence for such a "timer" can be found in SI Table S4, which lists the slope of linear regression for
472 Trt vs Tri plots in different growth conditions. As can be seen from SI Table S4, this slope is close to one
473 in slow growth conditions.

474 In the experiments, the replisome is imaged using a DnaN marker. The DnaN marker is expected to remain
475 attached to the replication terminus region after completion of replication [25]. Thus, in experiments the
476 measured time of termination Trt is,

$$477 \quad Trt = Trt' + Ta, \quad (2)$$

478 where Ta is the time for which DnaN stays attached. Ta is assumed to be exponentially distributed with
479 a mean time $\langle Ta \rangle = 3-6$ mins expected in our growth conditions [25].

480 We assume Tri to be normally distributed with mean $\langle Tri \rangle$ and standard deviation σ_{ri} , the values for
 481 which are determined from experiments. Assuming v to be normally distributed with a mean v_0 and
 482 standard deviation σ_v , the C period has an approximately normal distribution with mean $\langle C \rangle = \frac{N}{v_0}$ and
 483 variance $\sigma_C^2 = \left(\frac{N\sigma_v}{v_0^2}\right)^2$ when $\sigma_v \ll v_0$. Using Equations 1 and 2, we can determine $\langle C \rangle$ and σ_C^2 to be,

$$484 \quad \langle C \rangle = \langle Trt - Tri \rangle - \langle Ta \rangle, \quad (3)$$

$$485 \quad \sigma_C^2 = Var(Trt - Tri) - \langle Ta \rangle^2. \quad (4)$$

486 $\langle Trt - Tri \rangle$ and $Var(Trt - Tri)$ are the mean and variance of $Trt - Tri$ and are determined directly
 487 from experiments (SI Table S4).

488 In our model, constriction is said to be controlled by an event placed at a locus that is a relative distance
 489 of x from the replication terminus. $x = 0$ denotes the locus is at the terminus while $x = 1$ denotes a
 490 checkpoint at the initiation. Under the assumption that v has a Gaussian distribution with $CV \ll 1$, we
 491 obtain that the checkpoint is triggered after a time ξ from initiation which is normally distributed with
 492 mean

$$493 \quad \langle C \rangle(1 - x) = \frac{N(1-x)}{v_0} \text{ and variance } \sigma_C^2(1 - x)^2 = \left(\frac{N(1-x)\sigma_v}{v_0^2}\right)^2. \text{ Thus, the checkpoint is said to be reached}$$

494 at time Tx given by,

$$495 \quad Tx = Tri + \xi. \quad (5)$$

496 Since termination happens at a fraction x along the genome from Tx ,

$$497 \quad Trt' = Tx + \zeta, \quad (6)$$

498 where ζ is normally distributed with mean $\langle C \rangle x$ and variance $\sigma_C^2 x^2$. Note that ξ and ζ are correlated with
 499 each other with covariance $Cov(\xi, \zeta) = \sigma_C^2 x(1 - x)$. Both ξ and ζ are also correlated with the C period.

500 Constriction is assumed to be triggered by the checkpoint at time Tx at a constant rate r . This is based on
 501 the fact that the positive values of $Tn - Trt$ are exponentially distributed (Fig. 1D) and the CV of $Tn -$
 502 Trt is close to one (Fig. 2D). Hence, the time at constriction Tn is,

$$503 \quad Tn = Tx + Txn. \quad (7)$$

504 Txn is exponentially distributed with a mean time $= \frac{1}{r}$. Using eqs. 2 and 6, we get

505
$$\frac{1}{r} = \langle Tn - Trt \rangle + \langle Ta \rangle + \langle C \rangle x. \quad (8)$$

506 $\langle Tn - Trt \rangle$ can be determined from experiments thus fixing the rate r for different x . x is a free
507 parameter whose value is yet to be determined. Using the experimental results plotted in Fig. 2 and
508 comparing them against the analytical results for varying x , we obtain constraints on the value of x .

509 We shall first calculate analytically $CV(Tn - Trt)$ for a given value of x , which can be compared to
510 experimentally determined values shown in Fig. 2D. Using eqs. 2, 6, and 7, we get,

511
$$Tn - Trt = Txn - (\zeta + Ta). \quad (9)$$

512 Txn, ζ, Ta are independent of each other. Hence the variance of $Tn - Trt$ is

513
$$Var(Tn - Trt) = \left(\frac{1}{r}\right)^2 + \sigma_C^2 x^2 + \langle Ta \rangle^2, \quad (10)$$

514 while the mean is $\frac{1}{r} - (\langle C \rangle x + \langle Ta \rangle)$. Combining the two, we find:

515
$$CV(Tn - Trt) = \frac{\sqrt{\left(\frac{1}{r}\right)^2 + \sigma_C^2 \cdot x^2 + \langle Ta \rangle^2}}{\frac{1}{r} - \langle C \rangle x - \langle Ta \rangle}. \quad (11)$$

516 Other statistical constructs presented in Fig. 2 include the Pearson correlation coefficient for Trt, Tn ,
517 $R(Tn, Trt)$ and the slope of linear regression for Tn vs Trt plot.

518 $R(Tn, Trt)$ is defined as,

519
$$R(Tn, Trt) = \frac{\langle (Tn - \langle Tn \rangle)(Trt - \langle Trt \rangle) \rangle}{\sigma_{rt} \sigma_n}, \quad (12)$$

520 where σ_{rt} and σ_n are the standard deviations of Trt and Tn , respectively.

521 From eqs. 5 and 7, we obtain $Tn = Tri + Txn + \xi$. Similarly, from eqs. 1 and 2, $Trt = Tri + C + Ta$. All
522 pairs of variables from Tri, C, Ta, Txn, ξ are uncorrelated with each other except C and ξ which are
523 correlated as remarked earlier. Substituting this into eq. 12, we find the covariance (numerator) to be,

524
$$\begin{aligned} \langle (Tn - \langle Tn \rangle)(Trt - \langle Trt \rangle) \rangle &= \langle Tri^2 \rangle - \langle Tri \rangle^2 + \langle C\xi \rangle - \langle C \rangle \langle \xi \rangle \\ &= \sigma_{ri}^2 + \sigma_C^2 (1 - x). \end{aligned} \quad (13)$$

525 σ_n and σ_{rt} are found to be:

526
$$\sigma_n^2 = \sigma_{ri}^2 + \left(\frac{1}{r}\right)^2 + \sigma_c^2(1-x)^2, \quad (14)$$

527
$$\sigma_{rt}^2 = \sigma_{ri}^2 + \sigma_c^2 + \langle Ta \rangle^2. \quad (15)$$

528 Substituting eqs. 13, 14, and 15 into eq. 12, we can obtain $R(Tn, Trt)$. All the parameters in the formula
529 for $R(Tn, Trt)$ can be extracted from experiments while x is a variable.

530 The slope of the linear regression line for Tn vs Trt is related to $R(Tn, Trt)$ as

531
$$Slope(Tn, Trt) = \frac{R(Tn, Trt)\sigma_n}{\sigma_{rt}}. \quad (16)$$

532 This can also be calculated by substituting the values in eq. 13, 14, and 15. This theoretical prediction is
533 compared to the experimental data in Fig. 2C.

534 Assuming the trigger for the constriction event to be at termination (i.e., $x = 0$), we can obtain the
535 distribution of $Tn - Trt$ times analytically and compare it to experimental distributions. For $x = 0$, we
536 obtain $Tn - Trt = T_{xn} - Ta$. Let us define the random variable $Z = Tn - Trt$. We aim to find its
537 distribution. Using our assumptions that T_{xn} and Ta are independent and exponentially distributed, we
538 obtain the joint probability distribution of T_{xn} and Ta to be,

539
$$f(t_{xn}, t_a) = \frac{r}{\langle Ta \rangle} e^{-r t_{xn}} \cdot e^{-\frac{t_a}{\langle Ta \rangle}}. \quad (17)$$

540 For $z \geq 0$,

541
$$P_+(Z \leq z) = \frac{r}{\langle Ta \rangle} \int_0^\infty e^{-\frac{t_a}{\langle Ta \rangle}} dt_a \int_0^{t_a+z} e^{-r t_{xn}} dt_{xn} = 1 - \frac{e^{-rz}}{1 + r\langle Ta \rangle}, \quad (18)$$

542 with $P_+(Z \leq z)$ the cumulative distribution function (CDF) of Z for $z \geq 0$. Similarly, for $z \leq 0$, we obtain,

543
$$P_-(Z \leq z) = \frac{r}{\langle Ta \rangle} \int_{-z}^\infty e^{-\frac{t_a}{\langle Ta \rangle}} dt_a \int_0^{t_a+z} e^{-r t_{xn}} dt_{xn} = \frac{r\langle Ta \rangle}{1 + r\langle Ta \rangle} e^{\frac{z}{\langle Ta \rangle}}. \quad (19)$$

544 Therefore, we find that the probability distribution of $Z = Tn - Tri$, $g(z) = \frac{dP(z)}{dz}$ is

545
$$g(z) = \frac{1}{\frac{1}{r} + \langle Ta \rangle} \begin{cases} e^{-rz}, & z \geq 0 \\ e^{\frac{z}{\langle Ta \rangle}}, & z < 0 \end{cases}. \quad (20)$$

546 The parameters can be determined using the experimental data as discussed before.

547 Finally, we also investigate the relationship between replication initiation timing Tri and timing for
 548 initiation of constriction Tn . As before we will calculate the relevant statistics as a function of x . We will
 549 rely on the fact that $Tn = Tri + Txn + \xi$, and that Tri, Txn and ξ are uncorrelated. The variance of $Tn -$
 550 Tri is found to be,

$$551 \quad \text{Var}(Tn - Tri) = \left(\frac{1}{r}\right)^2 + \sigma_c^2 (1 - x)^2, \quad (21)$$

552 while the mean of $Tn - Tri = \frac{1}{r} + \langle C \rangle (1 - x)$. Thus, $\text{CV}(Tn - Tri)$ is found to be,

$$553 \quad \text{CV}(Tn - Tri) = \frac{\sqrt{\left(\frac{1}{r}\right)^2 + \sigma_c^2 (1 - x)^2}}{\frac{1}{r} + \langle C \rangle (1 - x)}. \quad (22)$$

554 Other statistical constructs which we calculate include the Pearson correlation coefficient for Tri, Tn ,
 555 $R(Tn, Tri)$ and the slope of linear regression for Tn vs Tri plot.

556 $R(Tn, Tri)$ is defined as,

$$557 \quad R(Tn, Tri) = \frac{\langle (Tn - \langle Tn \rangle)(Tri - \langle Tri \rangle) \rangle}{\sigma_{ri} \sigma_n}, \quad (23)$$

558 Using $Tn = Tri + Txn + \xi$, we find the numerator to be:

$$559 \quad \langle (Tn - \langle Tn \rangle)(Tri - \langle Tri \rangle) \rangle = \sigma_{ri}^2. \quad (24)$$

560 The quantity σ_{ri} is directly inferred from experiments while σ_n is calculated using eq. 14. Substituting the
 561 values into eq. 23, we can obtain $R(Tn, Tri)$. The slope of the linear regression line between Tn and Tri
 562 is related to $R(Tn, Tri)$ as

$$563 \quad \text{Slope}(Tn, Tri) = \frac{R(Tn, Tri) \sigma_n}{\sigma_{ri}} = 1. \quad (25)$$

564 Hence, the slope of the linear regression line for Tn vs Tri is always one independent of growth
 565 conditions. In other words, within the model Tn is related to Tri via a timer. In the four slowest growing
 566 conditions, the slope between Tn vs Tri is indeed close to 1 as shown in SI Fig. S5C.

References

1. Cooper, S., and Helmstetter, C.E. (1968). Chromosome replication and division cycle of *Escherichia coli* B/r. *Journal of Molecular Biology* 31, 519-540.
2. Wallden, M., Fange, D., Lundius, E.G., Baltekin, O., and Elf, J. (2016). The synchronization of replication and division cycles in individual *E. coli* cells. *Cell* 166, 729-739.
3. Amir, A. (2014). Cell size regulation in bacteria. *Phys. Rev. Lett.* 112, 208102.
4. Campos, M., Surovtsev, I.V., Kato, S., Paintdakhi, A., Beltran, B., Ebmeier, S.E., and Jacobs-Wagner, C. (2014). A constant size extension drives bacterial cell size homeostasis. *Cell* 159, 1433-1446.
5. Taheri-Araghi, S., Bradde, S., Sauls, J.T., Hill, N.S., Levin, P.A., Paulsson, J., Vergassola, M., and Jun, S. (2015). Cell-size control and homeostasis in bacteria. *Curr. Biol.* 25, 385-391.
6. Ho, P.-Y., and Amir, A. (2015). Simultaneous regulation of cell size and chromosome replication in bacteria. *Frontiers in Microbiology* 6, 662.
7. Witz, G., van Nimwegen, E., and Julou, T. (2019). Initiation of chromosome replication controls both division and replication cycles in *E. coli* through a double-adder mechanism. *Elife* 8, 48063.
8. Si, F.W., Le Treut, G., Sauls, J.T., Vadia, S., Levin, P.A., and Jun, S. (2019). Mechanistic origin of cell-size control and homeostasis in bacteria. *Curr. Biol.* 29, 1-11.
9. Bernander, R., and Nordstrom, K. (1990). Chromosome replication does not trigger cell division in *Escherichia coli*. *Cell* 60, 365-374.
10. Harris, L.K., and Theriot, J.A. (2016). Relative Rates of Surface and Volume Synthesis Set Bacterial Cell Size. *Cell* 165, 1479-1492.
11. Micali, G., Grilli, J., Marchi, J., Osella, M., and Lagomarsino, M.C. (2018). Dissecting the control mechanisms for DNA replication and cell division in *E. coli*. *Cell Reports* 25, 761-771.
12. Micali, G., Grilli, J., Osella, M., and Lagomarsino, M.C. (2018). Concurrent processes set *E. coli* cell division. *Science Advances* 4, aau3324.
13. Willis, L., and Huang, K.C. (2017). Sizing up the bacterial cell cycle. *Nat. Rev. Microbiol.* 15, 606-620.
14. Haeusser, D.P., and Margolin, W. (2016). Splitsville: structural and functional insights into the dynamic bacterial Z ring. *Nat. Rev. Microbiol.* 14, 305-319.
15. Aarsman, M.E.G., Piette, A., Fraipont, C., Vinkenvleugel, T.M.F., Nguyen-Disteche, M., and den Blaauwen, T. (2005). Maturation of the *Escherichia coli* divisome occurs in two steps. *Mol. Microbiol.* 55, 1631-1645.
16. Du, S.S., and Lutkenhaus, J. (2019). At the heart of bacterial cytokinesis: the Z ring. *Trends in Microbiology* 27, 781-791.
17. Männik, J., Walker, B.E., and Männik, J. (2018). Cell cycle-dependent regulation of FtsZ in *Escherichia coli* in slow growth conditions. *Mol. Microbiol.* 110, 1030-1044.
18. Walker, B.E., Mannik, J., and Mannik, J. (2020). Transient membrane-linked FtsZ assemblies precede Z-ring formation in *Escherichia coli*. *Curr. Biol.* 30, 499-508.
19. Liu, B., Persons, L., Lee, L., and de Boer, P.A.J. (2015). Roles for both FtsA and the FtsBLQ subcomplex in FtsN-stimulated cell constriction in *Escherichia coli*. *Mol. Microbiol.* 95, 945-970.

20. Egan, A.J.F., Errington, J., and Vollmer, W. (2020). Regulation of peptidoglycan synthesis and remodelling. *Nat. Rev. Microbiol.* *18*, 446-460.
21. Weiss, D.S. (2015). Last but not least: new insights into how FtsN triggers constriction during *Escherichia coli* cell division. *Mol. Microbiol.* *95*, 903-909.
22. Daley, D.O., Skoglund, U., and Soderstrom, B. (2016). FtsZ does not initiate membrane constriction at the onset of division. *Scientific Reports* *6*, srep33138.
23. Boes, A., Olatunji, S., Breukink, E., and Terrak, M. (2019). Regulation of the peptidoglycan polymerase activity of PBP1b by antagonist actions of the core divisome proteins FtsBLQ and FtsN. *MBio* *10*, 01912-01918.
24. Taguchi, A., Welsh, M.A., Marmont, L.S., Lee, W., Sjodt, M., Kruse, A.C., Kahne, D., Bernhardt, T.G., and Walker, S. (2019). FtsW is a peptidoglycan polymerase that is functional only in complex with its cognate penicillin-binding protein. *Nature Microbiology* *4*, 587-594.
25. Moolman, M.C., Krishnan, S.T., Kerssemakers, J.W.J., van den Berg, A., Tulinski, P., Depken, M., Reyes-Lamothe, R., Sherratt, D.J., and Dekker, N.H. (2014). Slow unloading leads to DNA-bound beta(2)-sliding clamp accumulation in live *Escherichia coli* cells. *Nature Communications* *5*, 11.
26. Reyes-Lamothe, R., Sherratt, D.J., and Leake, M.C. (2010). Stoichiometry and architecture of active DNA replication machinery in *Escherichia coli*. *Science* *328*, 498-501.
27. Soderstrom, B., Chan, H., Shilling, P.J., Skoglund, U., and Daley, D.O. (2018). Spatial separation of FtsZ and FtsN during cell division. *Mol. Microbiol.* *107*, 387-401.
28. Busiek, K.K., and Margolin, W. (2014). A role for FtsA in SPOR-independent localization of the essential *Escherichia coli* cell division protein FtsN. *Mol. Microbiol.* *92*, 1212-1226.
29. Wang, P., Robert, L., Pelletier, J., Dang, W.L., Taddei, F., Wright, A., and Jun, S. (2010). Robust growth of *Escherichia coli*. *Curr. Biol.* *20*, 1099-1103.
30. Yang, D., Jennings, A.D., Borrego, E., Retterer, S.T., and Männik, J. (2018). Analysis of factors limiting bacterial growth in PDMS mother machine devices. *Frontiers in Microbiology* *9*, 871.
31. Herendeen, S.L., Vanbogelen, R.A., and Neidhardt, F.C. (1979). Levels of major proteins of *Escherichia coli* during growth at different temperatures. *J. Bacteriol.* *139*, 185-194.
32. Männik, J., and Bailey, M.W. (2015). Spatial coordination between chromosomes and cell division proteins in *Escherichia coli*. *Frontiers in Microbiology* *6*, 306.
33. Bernhardt, T.G., and de Boer, P.A.J. (2005). SlmA, a nucleoid-associated, FtsZ binding protein required for blocking septal ring assembly over chromosomes in *E. coli*. *Mol. Cell* *18*, 555-564.
34. Espeli, O., Borne, R., Dupaigne, P., Thiel, A., Gigant, E., Mercier, R., and Boccard, F. (2012). A MatP-divisome interaction coordinates chromosome segregation with cell division in *E. coli*. *EMBO J.* *31*, 3198-3211.
35. Bailey, M.W., Bissichia, P., Warren, B.T., Sherratt, D.J., and Männik, J. (2014). Evidence for divisome localization mechanisms independent of the Min system and SlmA in *Escherichia coli*. *PLoS Genet.* *10*, 1004504.
36. Sherratt, D.J., Arciszewska, L.K., Crozat, E., Graham, J.E., and Grainge, I. (2010). The *Escherichia coli* DNA translocase FtsK. *Biochemical Society Transactions* *38*, 395-398.

37. Männik, J., Bailey, M.W., O'Neill, J.C., and Männik, J. (2017). Kinetics of large-scale chromosomal movement during asymmetric cell division in *Escherichia coli*. *PLoS Genet.* *13*, e1006638.
38. Cho, H.B., McManus, H.R., Dove, S.L., and Bernhardt, T.G. (2011). Nucleoid occlusion factor SlmA is a DNA-activated FtsZ polymerization antagonist. *Proc. Natl. Acad. Sci. U. S. A.* *108*, 3773-3778.
39. Stouf, M., Meile, J.-C., and Cornet, F. (2013). FtsK actively segregates sister chromosomes in *Escherichia coli*. *Proc. Natl. Acad. Sci. U. S. A.* *110*, 11157-11162.
40. Galli, E., Midonet, C., Paly, E., and Barre, F.X. (2017). Fast growth conditions uncouple the final stages of chromosome segregation and cell division in *Escherichia coli*. *PLoS Genet.* *13*, 1006702.
41. Barre, F.X., Aroyo, M., Colloms, S.D., Helfrich, A., Cornet, F., and Sherratt, D.J. (2000). FtsK functions in the processing of a Holliday junction intermediate during bacterial chromosome segregation. *Genes Dev.* *14*, 2976-2988.
42. Mulder, E., and Woldringh, C.L. (1989). Actively replicating nucleoids influence positioning of division sites in *Escherichia coli* filaments forming cells lacking DNA. *J. Bacteriol.* *171*, 4303-4314.
43. Cambridge, J., Blinkova, A., Magnan, D., Bates, D., and Walker, J.R. (2014). A replication-inhibited unsegregated nucleoid at mid-cell blocks Z-ring formation and cell division independently of SOS and the SlmA nucleoid occlusion protein in *Escherichia coli*. *J. Bacteriol.* *196*, 36-49.
44. Rodrigues, C.D.A., and Harry, E.J. (2012). The Min system and nucleoid occlusion are not required for identifying the division site in *Bacillus subtilis* but ensure its efficient utilization. *PLoS Genet.* *8*, 1002561.
45. Datsenko, K.A., and Wanner, B.L. (2000). One-step inactivation of chromosomal genes in *Escherichia coli* K-12 using PCR products. *Proc. Natl. Acad. Sci. U. S. A.* *97*, 6640-6645.
46. Cherepanov, P.P., and Wackernagel, W. (1995). Gene disruption in *Escherichia coli* - TcR and Km(R) cassettes with the option of flp-catalyzed excision of the antibiotic-resistance determinant. *Gene* *158*, 9-14.
47. Nicholls, A. (2014). Confidence limits, error bars and method comparison in molecular modeling. Part 1: The calculation of confidence intervals. *Journal of Computer-Aided Molecular Design* *28*, 887-918.